



Two-temperature activity induces liquid-crystal phases inaccessible in equilibrium

Jayeeta Chattopadhyay, Sriram Ramaswamy, Chandan Dasgupta , and Prabal K. Maiti*
 Centre for Condensed Matter Theory, Department of Physics, Indian Institute of Science, Bangalore 560012, India

 (Received 29 April 2022; accepted 17 January 2023; published 6 February 2023)

In equilibrium hard-rod fluids, and in effective hard-rod descriptions of anisotropic soft-particle systems, the transition from the isotropic (I) phase to the nematic phase (N) is observed above the rod aspect ratio $L/D = 3.70$ as predicted by Onsager. We examine the fate of this criterion in a molecular dynamics study of a system of soft repulsive spherocylinders rendered active by coupling half the particles to a heat bath at a higher temperature than that imposed on the other half. We show that the system phase-separates and self-organizes into various liquid-crystalline phases that are not observed in equilibrium for the respective aspect ratios. In particular, we find a nematic phase for $L/D = 3$ and a smectic phase for $L/D = 2$ above a critical activity.

DOI: [10.1103/PhysRevE.107.024701](https://doi.org/10.1103/PhysRevE.107.024701)

I. INTRODUCTION

The equilibrium liquid-crystalline properties of anisotropic particles are well understood [1–14]. Onsager’s theory [1] of the transition from the isotropic (I) phase to the nematic (N) phase, which has uniaxial apolar orientational order, predicts that a nematic phase cannot arise for hard rods with aspect ratio $L/D < 3.70$ [1–3]. In this paper, we inquire into the extension of Onsager’s limit to active matter, in the specific context of two-temperature systems.

Active matter is driven locally by a constant supply of free energy to its constituent particles, which dissipate it by performing mechanical work [15–37]. In flocking models, activity is linked to a vector order parameter [15–17,38,39]. In scalar active matter [31,40–43], activity enters by minimally breaking the detailed balance in scalar Halperin-Hohenberg models [44] or, as in our present work, by introducing two (or more) species of particles coupled to thermal baths at distinct temperatures [42,43,45–52]. The temperatures in question are not thermodynamic but emergent from the effective diffusivities of the multiple motile species. Two-temperature models have accounted for chromatin organization in the cell nucleus [47], self-organization in bidisperse Brownian soft disks [43] and Lennard-Jones (LJ) particles [50], and in polymer systems [48,49]. Recently, we have implemented this idea in a system of soft repulsive spherocylinders (SRSs) of aspect ratio $L/D = 5$ (where L and D are the effective length and diameter defined by the anisotropic repulsive potential [3,5,53–55]) and showed that increasing the temperature of the hot particles promotes liquid-crystal ordering in the cold particles, shifting the IN phase boundary to lower densities than its equilibrium location [51]. Here, we aim to explore ordering transitions of SRSs of different L/D , in particular, those below Onsager’s limit.

II. MODEL AND SIMULATION METHOD

We have carried out a series of molecular dynamics (MD) simulations of a system of SRSs with $L/D = 5, 3$, and 2. The model [Fig. 1(a)] and simulation protocol are as in our previous work [51]. Here, we give brief details for completeness. The SRSs interact through the Weeks-Chandler-Andersen potential [56]:

$$U_{\text{SRS}} = 4\epsilon \left[\left(\frac{D}{d_m} \right)^{12} - \left(\frac{D}{d_m} \right)^6 \right] + \epsilon \quad \text{if } d_m < 2^{\frac{1}{6}}D$$

$$= 0 \quad \text{if } d_m \geq 2^{\frac{1}{6}}D. \quad (1)$$

Here, d_m , the shortest distance between two spherocylinders, implicitly determines their relative orientation and the direction of the interaction force [3,5,53–55]. We build the initial configuration in a hexagonal-close-packed (HCP) crystal structure and perform MD simulations at constant particle number, pressure, and temperature (NPT) with periodic boundary conditions in all three directions [7,8,57]. For each aspect ratio, we simulate a wide range of pressures spanning the transition from the crystal to the isotropic phase and characterize the phases by calculating the nematic order parameter and appropriate pair correlation functions. For a system of N spherocylinders labeled $i = 1, \dots, N$, with orientations defined by unit vectors \mathbf{u}_i with components $u_{i\alpha}$, the traceless symmetric nematic order parameter \mathbf{Q} has components $Q_{\alpha\beta} = (1/N) \sum_{i=1}^N [(3/2)u_{i\alpha}u_{i\beta} - \frac{1}{2}\delta_{\alpha\beta}]$. The scalar nematic order parameter S is the largest eigenvalue of \mathbf{Q} .

Hereafter we work in reduced units defined in terms of the system parameters ϵ and D : temperature $T^* = k_B T / \epsilon$, pressure $P^* = P v_{\text{HSC}} / (k_B T)$, and packing fraction $\eta = v_{\text{HSC}} \rho$, where $\rho = N/V$ and $v_{\text{HSC}} = \pi D^2 (D/6 + L/4)$ is the volume of a spherocylinder.

Activity in our system is introduced by connecting half of the particles to a thermostat of higher temperature, while maintaining the temperature of the other half fixed at a lower value. Let T_h^* and T_c^* be the temperatures of the baths connected to the hot and cold particles, respectively, controlled by

*maiti@iisc.ac.in

TABLE I. Liquid-crystal phases in the cold zone for the respective aspect ratios at different activities. The phases that are absent in the equilibrium system and occur in the active systems are mentioned in bold. The equilibrium phases of HSC at the given aspect ratios are taken from Refs. [3,4].

A_{SRS}	A_{HSC}	$\chi = 0$	Phases at $\chi \neq 0$
5	5.28	I, N, Sm, K	I, N, Sm, K, multidomain K at $\eta = 0.36$
3	3.20	I, Sm, K	I, N, Sm, K at $\eta = 0.33$
2	2.11	I, K	I, Sm , K at $\eta = 0.45$

a Berendsen thermostat [58] with a time constant $\tau_T = 0.01$. We then define the activity $\chi = (T_h^* - T_c^*)/T_c^*$. Starting from a statistically isotropic structure at a definite temperature with $T_h^* = T_c^* = 5$, we gradually increase the temperature of the hot particles T_h^* , keeping the *volume* of the simulation box constant [51].

III. RESULTS

A. Equilibrium phase behavior of SRS and Onsager's limit

In equilibrium, we observe four stable phases for $L/D = 5$, crystal (K), smectic-A (SmA), nematic (N), and isotropic (I), three stable phases for $L/D = 3$, crystal, smectic-A, and isotropic, and two stable phases for $L/D = 2$, crystal and isotropic [see Fig. S1 in the Supplemental Material (SM) [59]]. Our results are consistent with the studies of soft rods [5,6].

To define a criterion analogous to that of Onsager [1] for our case, we construct an effective hard-cylinder diameter for the SRS, in terms of the interaction potential and the temperature of the system (Fig. S2) defined as $D_{\text{eff}}(T) = \int_0^\infty (1 - \exp[-\beta U_{\text{SRS}}(d_m)])d(d_m)$ [6,60,61]. Therefore, a SRS with aspect ratio $A_{\text{SRS}} = L/D$ can be mapped to a hard spherocylinder (HSC) with an effective aspect ratio $A_{\text{HSC}} = L/D_{\text{eff}}$. In Table I, we mention different values of A_{SRS} and the corresponding values of A_{HSC} at $T^* = 5$. The value of A_{SRS} corresponding to $A_{\text{HSC}} = 3.70$ (Onsager's limit for HSC) becomes $A_{\text{SRS}} = 3.52$ (Onsager's limit for SRS) at $T^* = 5$. This approximate version of Onsager's criterion is verified by the absence of a nematic phase for SRS at thermal equilibrium with $A_{\text{SRS}} = 3$ and 2 in our simulations and those of Cuetos *et al.* [5,6].

B. Activity-induced phase separation

Starting from a homogeneous isotropic structure, we observe local phase separation between hot and cold particles, which emerges at the macroscopic scale by forming a well-defined interface [Figs. 1(b)–1(e)]. We quantify the degree of mesoscale phase separation through the difference between the local densities of hot and cold particles. Dividing the simulation box into subcells labeled $i = 1, \dots, N_{\text{cell}}$ and letting $n_{\text{hot}}^i, n_{\text{cold}}^i$ be the numbers of hot and cold particles, respectively, in each cell, we define $\phi = N_{\text{cell}}^{-1} \langle \sum_{i=1}^{N_{\text{cell}}} |n_{\text{hot}}^i - n_{\text{cold}}^i| / n_{\text{tot}}^i \rangle$ [50,51] where the average $\langle \dots \rangle$ is carried out over a sufficiently large number of steady-state configurations. The choice of N_{cell} is such that

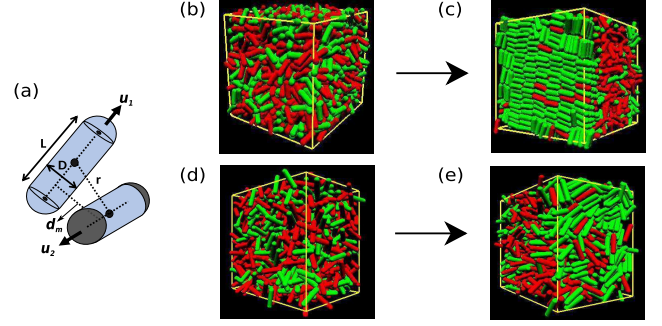


FIG. 1. (a) Schematic diagram of SRSs. The dotted line segment joining the centers of the two hemispheres is known as the core of the spherocylinder. \mathbf{u}_1 and \mathbf{u}_2 represent the orientation vectors of spherocylinders 1 and 2, respectively. r is the distance between their centers of mass, and d_m is the shortest distance that determines the interaction potential between them. (b)–(e) Snapshots representing steady-state configurations of hot (red) and cold (green) particles before (middle panel) and after (right panel) phase separation for the aspect ratios (b), (c) $L/D = 2$ at a packing fraction $\eta = 0.45$ and activity $\chi = 9$ and (d), (e) $L/D = 3$ at $\eta = 0.33$ and $\chi = 4$. Cold particles show (c) smectic ordering for $L/D = 2$ and (e) nematic ordering for $L/D = 3$ at the aforementioned activities.

each cell contains a sufficient number of particles to get stable statistics. ϕ is further offset by its initial value ϕ_0 at $\chi = 0$ [50,51].

In Fig. 2(a), we plot ϕ as a function of activity χ for $L/D = 5, 3$, and 2. For the sake of comparison, the system is chosen with a packing fraction between $\eta = 0.33$ and 0.36 for which the system is in the isotropic phase at thermal equilibrium for the given L/D at $T^* = 5$ (Fig. S1). From Fig. 2(a), we observe (i) phase separation starts at a lower activity for higher aspect ratios, and (ii) the amount of phase separation at a given χ is higher for higher aspect ratios. To understand observation (i) precisely, we calculate the critical activity χ_c , which is defined as the value of χ above which macroscopic phase separation is seen (see SM and Fig. S3 for details [59]). The calculated ranges of critical activities for the given packing fractions are $\chi_c = 1.4$ –2 for $L/D = 5$, $\chi_c = 2$ –3 for $L/D = 3$, and $\chi_c = 3$ –5 for $L/D = 2$.

C. Activity-induced liquid-crystalline ordering

After phase separation, the interactions between hot and cold particles mostly take place at the interface. The cold zone undergoes an ordering transition above a critical activity χ^* that depends on the aspect ratio of the rods as well as their packing fractions. In Fig. 2(b), we see that the nematic order parameter of cold particles S_{cold} increases with χ for $L/D = 5$ and 3 for $0 \leq \chi \leq 9$, while for $L/D = 2$ it increases above $\chi \geq 10$ (Fig. S4), resulting in a higher χ^* . However, the difference between the critical activities for phase separation and ordering decreases with increasing density. In Fig. 2(c), we have plotted S_{cold} vs χ for $L/D = 2$ at a slightly higher packing fraction, $\eta = 0.45$, which also corresponds to the isotropic phase in equilibrium. Here, we see both phase separation and the ordering transition for the given range of activities.

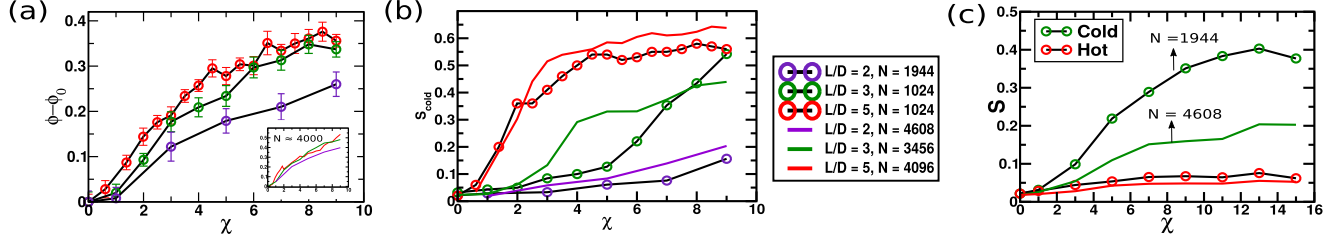


FIG. 2. (a) Density order parameter ϕ of the system and (b) nematic order parameter of the cold particles S_{cold} vs activity χ for different aspect ratios L/D at their respective packing fractions: for $L/D = 5$, $\eta = 0.36$, for $L/D = 3$, $\eta = 0.33$, and for $L/D = 2$, $\eta = 0.35$. (c) Nematic order parameter of the cold and hot particles for $L/D = 2$ at a higher packing fraction $\eta = 0.45$.

The critical activities for phase separation and ordering at $\eta = 0.45$ are $\chi_c = 3-5$ and $\chi^* = 5$, respectively.

The phases of the ordered structures in the cold zones are identified by calculating the local nematic order parameter S and appropriate pair correlation functions (see SM for details). We observe that with increasing activity both translational and orientational correlations in the cold zone are enhanced, indicating incipient order in the cold zone. Interestingly, we observe liquid-crystal phases for small values of L/D that do not occur for the same parameter range in a one-temperature system, i.e., in equilibrium.

In Figs. 3(a)–3(d), we plot different pair correlation functions of the cold particles at different activities for $L/D = 3$ at $\eta = 0.33$. We see that both translational $[g(r)]$ and orientational $[g_2(r)]$ pair correlation functions are flat in the absence of activity ($\chi = 0$) which is obvious for an isotropic phase. $g(r)$ develops the first peak at $\chi = 4$ and eventually the other peaks at higher values of χ . In Fig. 3(b), we see that $g_2(r)$ has a finite correlation length of roughly $2.5D$, beyond which it decays to zero for $\chi = 4$ and 5 and to a finite value for $\chi \geq 6$. This is also observed in the calculation of the half width at half maximum (HWHM) of $g_2(r)$ defined as the distance from the first peak at which the value of $g_2(r)$ is half of its value at the first peak (see Fig. S5 in SM for details). These observations suggest that there exists a finite orientational order in the cold zone for $\chi = 4$ and 5 which designates this phase as nematic. Above this activity, $g_2(r)$ develops multiple peaks at longer distances and saturates at a finite value. This is due to the presence of multiple clusters of different average directors, which effectively suppress the overall orientational correlation. In these cases, we calculate the $g_2(r)$ in a single cluster of a definite director and find it to saturate at a higher value, as shown

in the inset of Fig. 3(b). Smectic and crystalline structures are identified by calculating translational correlations along the parallel $[g_{\parallel}(r_{\parallel})]$ and perpendicular $[g_{\perp}(r_{\perp})]$ directions of the average nematic director of the spherocylinders. The periodic oscillations in $g_{\parallel}(r_{\parallel})$ and the liquidlike structure in $g_{\perp}(r_{\perp})$ at $\chi = 6$ and 7 indicate that the phase is smectic, as shown in Figs. 3(c) and 3(d).

Similarly, we find that the system with $L/D = 2$ exhibits smectic ordering at $\eta = 0.45$, $\chi = 9$ as shown in Fig. S6. However, the hot zone shows an isotropic structure with reduced packing fractions for each of the cases. Table I summarizes these results, comparing equilibrium and two-temperature phases for each aspect ratio.

D. Pressure anisotropy and heat flux

To find the microscopic origin of the ordering transitions that are not observed in equilibrium, we calculate the local pressure in the phase-separated system. We divide the simulation box into a number of slabs (i) along the direction normal to the interface, following the procedure mentioned in Ref. [51]. The region where the local densities of hot and cold particles change sharply between their values in the segregated zones is identified as the interfacial region [Fig. 4(a)].

We then calculate the pressure components along the normal (x) and tangential directions (yz) of the interfacial plane using the diagonal components of the stress tensor. Therefore, the normal P_n and tangential P_t components of the pressure are defined as $P_n(i) = P_{xx}(i)$ and $P_t(i) = [P_{yy}(i) + P_{zz}(i)]/2$, where $P_{\alpha\beta}(i) = \frac{1}{V(i)} (\sum_{j=1}^{n(i)} m v_j^\alpha v_j^\beta + \sum_{j=1}^{n(i)-1} \sum_{k>j} r_{jk}^\alpha f_{jk}^\beta)$. The first and second terms in this equation represent the

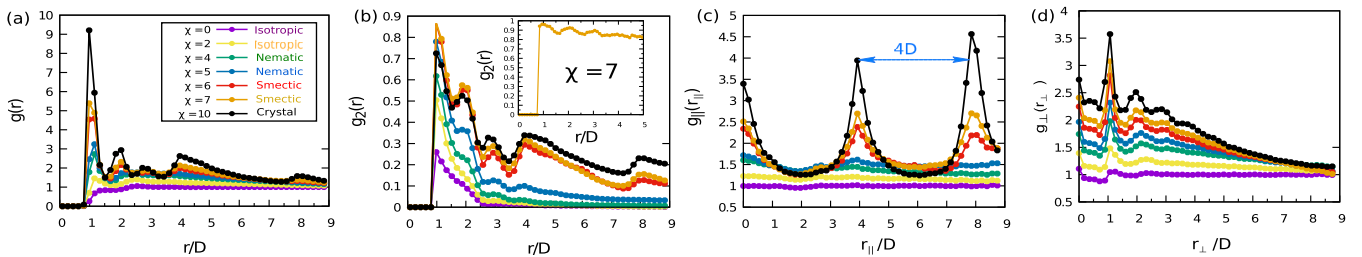


FIG. 3. Pair correlation functions for the cold particles at different activities χ for $L/D = 3$ at the packing fraction $\eta = 0.33$. (a) The center-of-mass pair radial distribution function $g(r)$, (b) orientational pair distribution function $g_2(r)$, and (c) projection of $g(r)$ along the direction parallel $[g_{\parallel}(r_{\parallel})]$ and (d) perpendicular $[g_{\perp}(r_{\perp})]$ to the director of the spherocylinders. The inset of (b) shows $g_2(r)$ at $\chi = 7$ in a single cluster with a definite director. The distance between the two peaks in (c) is $4D$, which is the end-to-end distance of a spherocylinder with $L/D = 3$.

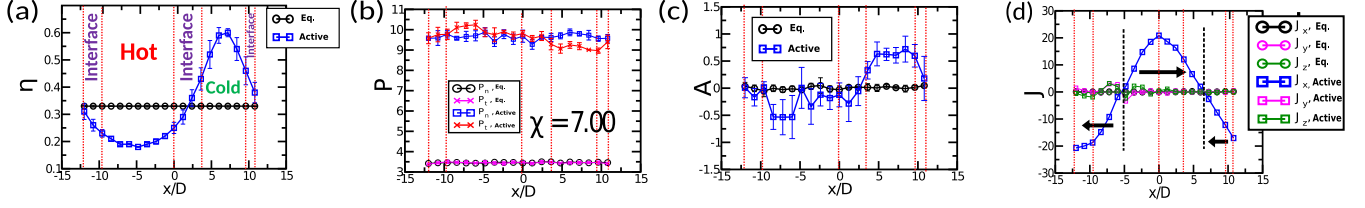


FIG. 4. Pressure anisotropy and local heat flux across the hot-cold interface for $L/D = 3$ at $\eta = 0.33$ and $\chi = 7$. We plot (a) effective packing fraction η , (b) normal (P_n) and tangential (P_t) components of the pressure, (c) pressure anisotropy $A = P_n - P_t$, and (d) local heat flux J along the direction perpendicular to the interfacial plane. The red dashed lines indicate boundaries of different zones. The black dashed lines in (d) indicate the location where the heat flux becomes 0. The arrows indicate the directions of the heat flow, depending on the sign of J . We find a positive pressure anisotropy at the interface that extends in the cold zone and a finite heat flux flowing from the bulk hot zone to the bulk cold zone. Here, $S_{\text{cold}} = 0.42$, $S_{\text{hot}} = 0.07$.

kinetic and virial contributions (arising due to the particle's interaction) of the pressure tensor, where $\vec{r}_j = (r_j^\alpha)$ and $\vec{v}_j = (v_j^\alpha)$ are the position and velocity of the j th particle ($\alpha = x, y, z$) and r_{jk} and \vec{f}_{jk} are the relative distance and interacting force between the SRSs j and k . $n(i)$ and $V(i)$ represent the total number of particles and volume of the i th slab.

In Fig. 4(b), for aspect ratio $L/D = 3$, we find the following: (i) In equilibrium ($\chi = 0$), normal and tangential pressure components are equal, implying that the pressure tensor is isotropic throughout the simulation box. (ii) After phase separation ($\chi \geq \chi_c$), the pressure anisotropy $A = P_n - P_t$ vanishes within error bars in the hot zone. (iii) At the interface and in the cold zone, P_t acquires a lower value, while P_n remains balanced throughout the simulation box. This causes a pressure anisotropy at the interface that persists in the bulk cold zone as well [Fig. 4(c)]. This compresses the cold zone along the interface normal promoting cold-particle alignment parallel to the interfacial plane, thereby inducing an ordering transition.

To understand further the effects of the activity, we calculate the local heat flux \vec{J} in each slab using the following equation [62,63],

$$\vec{J}(i) = \frac{1}{V(i)} \left\langle \sum_{j=1}^{n(i)} \vec{v}_j e_j + \sum_{j=1}^{n(i)} \sigma_j \cdot \vec{v}_j \right\rangle, \quad (2)$$

where $e_j = (1/2)mv_j^2 + \sum_{j \neq k} U_{jk}$ is the total energy and $\sigma_j = (1/2) \sum_{j \neq k} r_{jk} \vec{f}_{jk}$ is the stress tensor. In Fig. 4(d), we show the spatial variation of \vec{J} along the direction normal to the interface. We find $\vec{J} = 0$ in equilibrium, but it obtains a finite value in the phase-separated systems, both at the interface and in the bulk region. This reveals that, though the interaction between hot and cold particles takes place mainly at the interface, its effect extends to the bulk region as well. The sign of \vec{J} indicates heat flows from the bulk hot to the bulk cold zone. This results in heterogeneous activity and broken time-reversal invariance throughout the simulation box, giving rise to anomalous thermodynamic behavior (such as pressure anisotropy) away from the interface.

E. System size effects

For larger system sizes with $N \approx 4000$, we find S_{cold} saturates at a lower value for $L/D = 2$ [Fig. 2(c)] which is due

to the presence of multiple clusters that sometimes makes it challenging to identify the phases precisely. However, our key findings, i.e., the emergence of liquid-crystalline phases for the lower aspect ratios and the spontaneous appearance of macroscopic heat currents and anisotropic stresses in the bulk zones, remain unaffected by the system sizes (see Fig. 2 and Figs. S8–S11).

IV. CONCLUSION AND OUTLOOK

Our simulation study examines the effect of two-temperature activity in a soft-rod fluid for a range of effective aspect ratios of the rods. We show that the two-temperature model can give rise to liquid-crystal phases that are not observed in equilibrium for the respective aspect ratios. We observe a smectic phase for $L/D = 2$ and a nematic phase for $L/D = 3$. We find that the presence of two temperatures causes a pressure anisotropy extending from the hot-cold interface into the bulk of the cold zone, and a heat current flowing from the hot to the cold zone. Thus, the nonequilibrium behavior is not limited to the hot-cold interfaces but pervades the system as a whole, driving the anomalous ordering transitions in the cold zone. An understanding of these results within analytical theory, experimental realizations of two-temperature systems, presumably in suspensions with bidisperse motility, and methods to capture and stabilize the anomalously ordered domains are some of the challenges that emerge from our work.

ACKNOWLEDGMENTS

We would like to thank Prof. Aparna Baskaran for helpful discussions. We thank SERB, India for financial support through providing the computational facility. J.C. acknowledges support through an INSPIRE fellowship. J.C. thanks Tarun Maity, Subhadeep Dasgupta, and S. J. Kole for insightful discussions. S.R. was supported by a J. C. Bose Fellowship of the SERB, India, and by the Tata Education and Development Trust, and acknowledges discussions during the KITP 2020 online program on Symmetry, Thermodynamics and Topology in Active Matter. This research was supported in part by the National Science Foundation under Grant No. NSF PHY-1748958. C.D. was supported by a Distinguished Fellowship of the SERB, India.

- [1] L. Onsager, *Ann. N.Y. Acad. Sci.* **51**, 627 (1949).
- [2] P.-G. de Gennes and J. Prost, *The Physics of Liquid Crystals* (Oxford University Press, Oxford, U.K., 1993), Vol. 83.
- [3] P. Bolhuis and D. Frenkel, *J. Chem. Phys.* **106**, 666 (1997).
- [4] S. C. McGrother, D. C. Williamson, and G. Jackson, *J. Chem. Phys.* **104**, 6755 (1996).
- [5] A. Cuetos, B. Martínez-Haya, L. Rull, and S. Lago, *J. Chem. Phys.* **117**, 2934 (2002).
- [6] A. Cuetos and B. Martínez-Haya, *Mol. Phys.* **113**, 1137 (2015).
- [7] P. K. Maiti, Y. Lansac, M. A. Glaser, and N. A. Clark, *Phys. Rev. Lett.* **88**, 065504 (2002).
- [8] Y. Lansac, P. K. Maiti, N. A. Clark, and M. A. Glaser, *Phys. Rev. E* **67**, 011703 (2003).
- [9] D. Thirumalai, *J. Chem. Phys.* **84**, 5869 (1986).
- [10] H. Graf and H. Löwen, *Phys. Rev. E* **59**, 1932 (1999).
- [11] V. F. D. Peters, M. Vis, H. H. Wensink, and R. Tuinier, *Phys. Rev. E* **101**, 062707 (2020).
- [12] V. F. D. Peters, M. Vis, A. G. García, H. H. Wensink, and R. Tuinier, *Phys. Rev. Lett.* **125**, 127803 (2020).
- [13] A. Stroobants, H. Lekkerkerker, and T. Odijk, *Macromolecules* **19**, 2232 (1986).
- [14] D. Rajendra, J. Mandal, Y. Hatwalne, and P. K. Maiti, *Soft Matter* **19**, 137 (2023).
- [15] M. C. Marchetti, J. F. Joanny, S. Ramaswamy, T. B. Liverpool, J. Prost, M. Rao, and R. A. Simha, *Rev. Mod. Phys.* **85**, 1143 (2013).
- [16] S. Ramaswamy, *Annu. Rev. Condens. Matter Phys.* **1**, 323 (2010).
- [17] J. Toner, Y. Tu, and S. Ramaswamy, *Ann. Phys.* **318**, 170 (2005).
- [18] P. Romanczuk, M. Bär, W. Ebeling, B. Lindner, and L. Schimansky-Geier, *Eur. Phys. J.: Spec. Top.* **202**, 1 (2012).
- [19] J. Prost, F. Jülicher, and J.-F. Joanny, *Nat. Phys.* **11**, 111 (2015).
- [20] S. Ramaswamy, *Nat. Rev. Phys.* **1**, 640 (2019).
- [21] G. Gompper, R. G. Winkler, T. Speck, A. Solon, C. Nardini, F. Peruani, H. Löwen, R. Golestanian, U. B. Kaupp, L. Alvarez *et al.*, *J. Phys.: Condens. Matter* **32**, 193001 (2020).
- [22] R. A. Simha and S. Ramaswamy, *Phys. Rev. Lett.* **89**, 058101 (2002).
- [23] M. J. Bowick, N. Fakhri, M. C. Marchetti, and S. Ramaswamy, *Phys. Rev. X* **12**, 010501 (2022).
- [24] H. H. Wensink, J. Dunkel, S. Heidenreich, K. Drescher, R. E. Goldstein, H. Löwen, and J. M. Yeomans, *Proc. Natl. Acad. Sci. USA* **109**, 14308 (2012).
- [25] A. Doostmohammadi, J. Ignés-Mullol, J. M. Yeomans, and F. Sagués, *Nat. Commun.* **9**, 3246 (2018).
- [26] K. Thijssen, M. R. Nejad, and J. M. Yeomans, *Phys. Rev. Lett.* **125**, 218004 (2020).
- [27] A. Maitra and R. Voituriez, *Phys. Rev. Lett.* **124**, 048003 (2020).
- [28] M. R. Nejad and J. M. Yeomans, *Phys. Rev. Lett.* **128**, 048001 (2022).
- [29] I. Buttinoni, J. Bialké, F. Kümmel, H. Löwen, C. Bechinger, and T. Speck, *Phys. Rev. Lett.* **110**, 238301 (2013).
- [30] J. Bialké, J. T. Siebert, H. Löwen, and T. Speck, *Phys. Rev. Lett.* **115**, 098301 (2015).
- [31] A. V. Ivlev, J. Bartnick, M. Heinen, C.-R. Du, V. Nosenko, and H. Löwen, *Phys. Rev. X* **5**, 011035 (2015).
- [32] C. Bechinger, R. Di Leonardo, H. Löwen, C. Reichhardt, G. Volpe, and G. Volpe, *Rev. Mod. Phys.* **88**, 045006 (2016).
- [33] S. Mandal, B. Liebchen, and H. Löwen, *Phys. Rev. Lett.* **123**, 228001 (2019).
- [34] H. Löwen, *J. Chem. Phys.* **152**, 040901 (2020).
- [35] T. Speck, J. Bialké, A. M. Menzel, and H. Löwen, *Phys. Rev. Lett.* **112**, 218304 (2014).
- [36] S. R. McCandlish, A. Baskaran, and M. F. Hagan, *Soft Matter* **8**, 2527 (2012).
- [37] G. S. Redner, M. F. Hagan, and A. Baskaran, *Phys. Rev. Lett.* **110**, 055701 (2013).
- [38] T. Vicsek and A. Zafeiris, *Phys. Rep.* **517**, 71 (2012).
- [39] J. Toner and Y. Tu, *Phys. Rev. Lett.* **75**, 4326 (1995).
- [40] R. Wittkowski, A. Tiribocchi, J. Stenhammar, R. J. Allen, D. Marenduzzo, and M. E. Cates, *Nat. Commun.* **5**, 4351 (2014).
- [41] S. Saha, J. Agudo-Canalejo, and R. Golestanian, *Phys. Rev. X* **10**, 041009 (2020).
- [42] A. Y. Grosberg and J.-F. Joanny, *Phys. Rev. E* **92**, 032118 (2015).
- [43] S. N. Weber, C. A. Weber, and E. Frey, *Phys. Rev. Lett.* **116**, 058301 (2016).
- [44] P. C. Hohenberg and B. I. Halperin, *Rev. Mod. Phys.* **49**, 435 (1977).
- [45] A. Y. Grosberg and J.-F. Joanny, *Polym. Sci., Ser. C* **60**, 118 (2018).
- [46] E. Ilker and J.-F. Joanny, *Phys. Rev. Res.* **2**, 023200 (2020).
- [47] N. Ganai, S. Sengupta, and G. I. Menon, *Nucleic Acids Res.* **42**, 4145 (2014).
- [48] J. Smrek and K. Kremer, *Phys. Rev. Lett.* **118**, 098002 (2017).
- [49] J. Smrek and K. Kremer, *Entropy* **20**, 520 (2018).
- [50] S. S. N. Chari, C. Dasgupta, and P. K. Maiti, *Soft Matter* **15**, 7275 (2019).
- [51] J. Chattopadhyay, S. Pannir-Sivajothi, K. Varma, S. Ramaswamy, C. Dasgupta, and P. K. Maiti, *Phys. Rev. E* **104**, 054610 (2021).
- [52] N. Venkatareddy, S.-T. Lin, and P. K. Maiti, [arXiv:2109.00415](https://arxiv.org/abs/2109.00415).
- [53] M. P. Allen, G. T. Evans, D. Frenkel, and B. Mulder, *Adv. Chem. Phys.* **86**, 1 (1993).
- [54] C. Vega and S. Lago, *Comput. Chem. (Oxford, UK)* **18**, 55 (1994).
- [55] D. J. Earl, J. Ilnytskyi, and M. R. Wilson, *Mol. Phys.* **99**, 1719 (2001).
- [56] J. D. Weeks, D. Chandler, and H. C. Andersen, *J. Chem. Phys.* **54**, 5237 (1971).
- [57] M. Rotunno, T. Bellini, Y. Lansac, and M. A. Glaser, *J. Chem. Phys.* **121**, 5541 (2004).
- [58] H. J. Berendsen, J. v. Postma, W. F. van Gunsteren, A. DiNola, and J. R. Haak, *J. Chem. Phys.* **81**, 3684 (1984).
- [59] See Supplemental Material at <http://link.aps.org/supplemental/10.1103/PhysRevE.107.024701> for additional details on the pair correlation functions, critical activity, and the results for larger system sizes that support the main findings of the paper.
- [60] A. Cuetos, B. Martinez-Haya, S. Lago, and L. Rull, *J. Phys. Chem. B* **109**, 13729 (2005).
- [61] T. Boublík, *Mol. Phys.* **32**, 1737 (1976).
- [62] J.-P. Hansen and I. R. McDonald, *Theory of Simple Liquids: With Applications to Soft Matter* (Academic, Cambridge, MA, 2013).
- [63] P. J. Bhuyan, R. Mandal, P. Chaudhuri, A. Dhar, and C. Dasgupta, *Phys. Rev. E* **101**, 022125 (2020).